PCP
PLANT & CELL PHYSIOLOGY

Light Sheet Fluorescence Microscopy Quantifies Calcium Oscillations in Root Hairs of *Arabidopsis thaliana*

Alessia Candeo[1], Fabrizio G. Doccula[2], Gianluca Valentini[1], Andrea Bassi[1,*] and Alex Costa[2,*]

[1]Dipartimento di Fisica, Politecnico di Milano, Piazza Leonardo da Vinci 32, 20133 Milano, Italy
[2]Dipartimento di Bioscienze, Università degli Studi di Milano, Via Giovanni Celoria 26, 20133 Milano, Italy
*Corresponding authors: Alex Costa, E-mail, alex.costa@unimi.it; Fax, +390250314815; Andra Bassi, E-mail, andreabassi@polimi.it; Fax, +390223996126.

Calcium oscillations play a role in the regulation of the development of tip-growing plant cells. Using optical microscopy, calcium oscillations have been observed in a few systems (e.g. pollen tubes, fungal hyphae and algal rhizoids). High-resolution, non-phototoxic and rapid imaging methods are required to study the calcium oscillation in root hairs. We show that light sheet fluorescence microscopy is optimal to image growing root hairs of *Arabidopsis thaliana* and to follow their oscillatory tip-focused calcium gradient. We describe a protocol for performing live imaging of root hairs in seedlings expressing the cytosol-localized ratiometric calcium indicator Yellow Cameleon 3.6. Using this protocol, we measured the calcium gradient in a large number of root hairs. We characterized their calcium oscillations and correlated them with the rate of hair growth. The method was then used to screen the effect of auxin on the properties of the growing root hairs.

Keywords: Arabidopsis thaliana • Calcium oscillations • Cameleon calcium probe • Light sheet fluorescence microscopy • Root hairs.

Abbreviations: CCD, charge-coupled device; CFP, cyan fluorescent protein; CMOS, complementary metal-oxide semiconductor; FEP, fluorinated ethylene propylene; FRET, Förster resonance energy transfer; HF, high frequency; LF, low frequency; LSFM, light sheet fluorescence microscopy; MIP, maximum intensity projection; MS, Murashige and Skoog; NA, numerical aperture; NAA, 1-naphthaleneacetic acid; NES YC3.6, nuclear export signal Yellow Cameleon 3.6; PSD, power spectral density; ROI, region of interest.

Introduction

Tip growth is a highly specific and conserved developmental process that, in plants, governs both root hair and pollen tube elongation (Feijo et al. 2004, Campanoni and Blatt 2007). Tip growth is restricted to the very apex of the tubular growing structure. A complex pathway leads to growth of cell walls at the tip: new cell wall material is delivered and exported at the growing apex while outward-facing turgor pressure allows the cell to elongate (e.g. pollen and root hair cells) (Michard et al. 2009, Balcerowicz et al. 2015, Mendrinna and Persson 2015).

Tip growth typically occurs in an oscillating manner, with alternating periods of slower and faster growth. The frequency and amplitude of oscillations depend on environmental conditions and a highly organized interplay between gene transcription, protein turnover and modification, the cytoskeleton, the cell wall and membrane-localized import and export proteins (Rounds and Bezanilla 2013, Grierson et al. 2014, Mendrinna and Persson 2015). One of the key features of tip growth elongation is the steep tip-focused oscillating calcium gradient (Felle and Hepler 1997, Holdaway-Clarke et al. 1997, Franklin-Tong et al. 1999, Monshausen et al. 2007, Monshausen et al. 2008, Yan et al. 2009, Konrad et al. 2011).

Tip calcium oscillations in apical-growing cells have been characterized mainly in pollen tubes, fungal hyphae, algal rhizoids and, rarely, in root hairs (Felle and Hepler 1997, Holdaway-Clarke et al. 1997, Franklin-Tong et al. 1999, Monshausen et al. 2007, Coelho et al. 2008, Monshausen et al. 2008, Yan et al. 2009, Kim et al. 2012, Lange and Peiter 2016). Root hairs arise from the root epidermis, where they drastically increase the absorption area (Balcerowicz et al. 2015). In root hairs, the tip calcium gradient (Wymer et al. 1997, Monshausen et al. 2007, Monshausen et al. 2008) is maintained by an influx of extracellular calcium through hyperpolarization-activated calcium channels (Very and Davies 2000) that are active only at the extreme tip of growing hairs (Very and Davies 2000, Foreman et al. 2003). Studies of the root hairs from leguminosae species (e.g. *Medicago truncatula* and *Lotus japonicus*) have measured nuclear calcium oscillations in response to both rhizobia and mycorrhiza infections (reviewed in Charpentier and Oldroyd 2013). The work by Monshausen et al. (2008) is one of the first studies that reports the time-lapse analysis of tip calcium oscillations, providing information about their frequency and amplitude properties in growing healthy hairs.

The in vivo imaging of calcium concentrations and dynamics in biological specimens (and also in root hairs) has mainly relied on the use of dyes (e.g Indo-1-dextran) or genetically encoded sensors (e.g. Cameleon, GECOs) coupled with standard fluorescence microscopy techniques (e.g. wide-field fluorescence and confocal laser scanning microscopy) (Gilroy 1997, Wymer et al. 1997, Swanson et al. 2011, Okumoto et al. 2012, Costa et al. 2013, Costa and Kudla 2015, Keinath et al. 2015). However, standard microscopy techniques present several constraints that limit their applicability in the study of complex tissues,

such as plant roots and root hairs (Maizel et al. 2011, Costa et al. 2013). Wide-field epifluorescence microscopy has no sectioning capability and, as a consequence, in many cases the overwhelming signal generated by the entire primary root hinders the detection of the signal emitted by the root hairs, and may thus limit the dynamic range of measurements. Single-cell resolution can be obtained using confocal microscopy, spinning disk and multiphoton platforms. However, a high level of photodamage is a limitation for long-term imaging experiments, and measurements are thus confined to small volumes when fast sampling is required (Kao and Chen 2002, Monshausen et al. 2008). Moreover, during standard imaging procedures with classical fluorescence microscopy, the specimens are normally transferred to microscope slides and are placed horizontally, which compromises the growth of plant roots that are influenced by gravity (Band et al. 2012) and the hairs of which develop in a three-dimensional (3D) manner.

One solution to overcome most of these limitations is offered by light sheet fluorescence microscopy (LSFM), a technique that allows the rapid acquisition of images with a high dynamic range with single-cell resolution over a wide field of view and that can be easily tailored to a given specimen, including vertically growing seedlings (Maizel et al. 2011, Costa et al. 2013, Berthet and Maizel 2016). One of the advantages of LSFM is the low dose of light needed to image one plane, which enables long-term time-lapse imaging and the study of developmental processes (Bassi et al. 2015, Berthet and Maizel 2016). Such a fundamental advantage is reached because the sample is illuminated on one side and fluorescence is collected perpendicular to the illumination axis. This eliminates out-of-focus illumination, allows rapid acquisition with wide field detectors [charge-coupled device (CCD) or complementary metal-oxide semiconductor (CMOS) cameras] and drastically reduces phototoxicity.

We have recently reported that LSFM can be employed to study calcium dynamics in root cells (Costa et al. 2013) by analysing Arabidopsis plants expressing the Yellow Cameleon YC3.6 (Nagai et al. 2004). The Cameleon YC3.6 requires a single excitation and the simultaneous acquisition of two independent fluorescence emissions [cpVenus and cyan fluorescent protein (CFP)] which are used to calculate a ratio proportional to the calcium concentration (Miyawaki et al. 1997, Nagai et al. 2004). The combination of LSFM with the use of a plant expressing the Cameleon sensor provides a means for the study of root hair development, for simultaneous measurement of growth rate and calcium oscillations.

In this work, we characterize the spontaneous calcium oscillations in *Arabidopsis thaliana* root hairs and we correlate these oscillations with their growth. This was possible using LSFM and by implementing a protocol to perform live imaging of plants in close to physiological conditions. We present details on: (i) tailoring LSFM to ratiometric imaging of root hairs; (ii) specimen preparation; (iii) the design of the experiment; and (iv) data analysis. This method allowed us to produce statistically significant data of the calcium oscillations in the root hairs of wild-type plants and to study the effect of auxin on root hair growth together with its influence on tip calcium oscillations.

Results

Light sheet fluorescence microscopy allows imaging of the untouched plant

Germinated seedlings of the Arabidopsis Columbia (Col-0) line expressing the cytosolic localized Förster Resonance energy transfer (FRET) sensor Yellow Cameleon NES-YC3.6 (Krebs et al. 2012) were transferred just after seed germination (evaluated as rupture of the tegument and primary root emergence) from a Petri dish agar plate to the top of fluorinated ethylene propylene (FEP) tubes filled with a jellified medium (with 0.5% Phytagel™). FEP has a refractive index close to that of water (n_{FEP} = 1.344, n_{WATER} = 1.33) and avoids the strong optical aberrations associated with plastic or glass tubes. In this step, we selected healthy and fluorescent seedlings that were able to grow directly inside the tube, with their roots following positive gravitropism (**Fig. 1A–E**). The root and root hairs can grow for days in close to physiological conditions and can be imaged whenever suitable. Notably, this mounting procedure represents an added value and a considerable benefit for imaging analyses since it almost eliminates sample manipulation that is required for traditional root imaging (Behera and Kudla 2013, Loro and Costa 2013) and therefore reduces possible artifacts or tissue damage. When the seedlings were at the desired stage of development, the FEP tubes with the growing seedlings were coupled with a hollow aluminum holder and transferred to the imaging chamber of the LSFM set-up (Supplementary Fig. S1). We observed areas of around $800 \times 450\,\mu m^2$ for both fluorescent channels (cpVenus and CFP), which were recorded simultaneously on the same CMOS sensor, enabling us to calculate the signal of the FRET ratio (computed as the cpVenus/CFP ratio) in real time (**Fig. 1H**). As seen in the representative image shown in **Fig. 1F**, the microscope field of view was sufficient to observe a large part of the Arabidopsis root as well as protruding root hairs at young and adult stages. We could routinely perform morphological screening of Arabidopsis roots, in which multiple root hairs (>20) from the differentiation zone were detected in a single 3D measurement (**Fig. 1F–H**). To obtain the best 3D reconstructions, a spacing between slices equal to or lower than half of the light sheet thickness is recommended, particularly if deconvolution algorithms will be applied to the acquired image stack. We found in practice that a spacing comparable with the thickness of the light sheet was a good trade-off between image quality, light dose and data set size.

Growing root hairs show spontaneous calcium oscillations

In order to monitor the growth of root hair during time-lapse experiments, the bleaching of the calcium indicator (NES-YC3.6) had to be reduced as much as possible, especially for long-term analysis of single cells. Reduced bleaching was achieved by selecting the spacing between slices (which sets the light dose and the acquisition speed). As mentioned before, a spacing comparable with the thickness of the light sheet is a good trade-off. After setting up the image acquisition and processing protocol, we studied the link between calcium
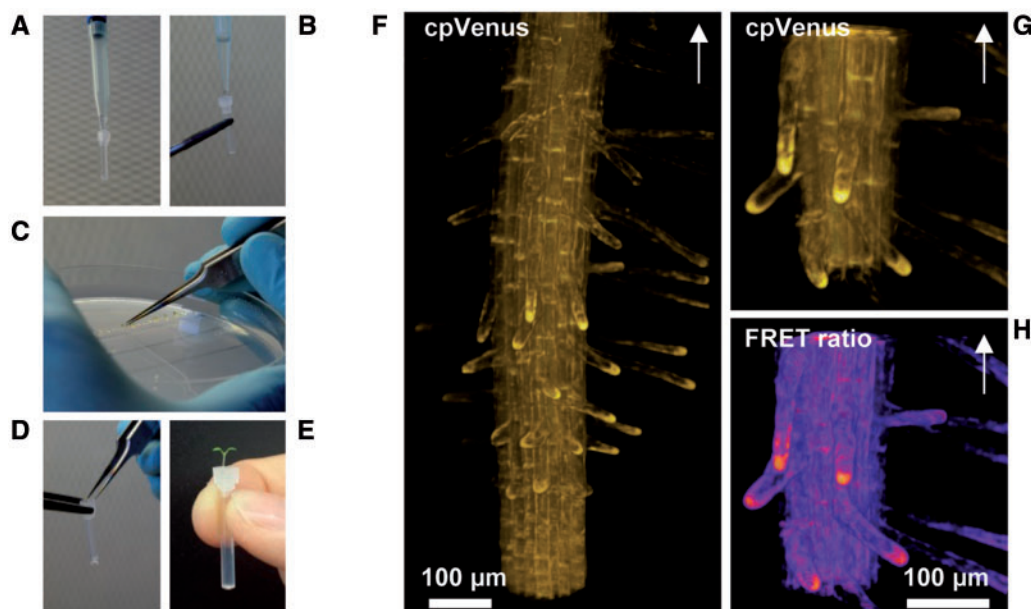
Fig. 1 Close to physiological mounting procedure for 3D imaging of Arabidopsis seedling roots. After cleaning, FEP tubes were coupled with the upper part of a 10 μl pipette tip and filled with a Phytagel™-based solution (A). A layer of agarose-based solution was then placed on top of the tube (B), where the seedlings were placed (D) after germination in Petri dishes (C). The roots grew inside the jelly matrix (E), and developing root hairs could be imaged thorough the FEP tube. Three-dimensional reconstructions of Arabidopsis root expressing the cytosolic-targeted Cameleon NES-YC3.6. Slices were acquired with a step of 1.5 μm. The single channel reconstruction (F) shows the root hairs three-dimensionally organized around the mature zone. Root hairs look straight, smooth and usually follow gravitropism, as shown in detail in (G). The same consideration can be made by looking at the FRET reconstruction (H). The arrow in (F–H) indicates the shoot position.

dynamics in the root hair apices and their growth. Thus, we imaged the Arabidopsis root hairs in 3D time-lapse experiments over different time scales and monitored the cpVenus and CFP fluorescence.

As first, we followed root hair development during 5 h, recording one entire volume stack (100 planes with a spacing of 3 μm) every 3 min. The laser power was set to 20 μW at the sample to limit phototoxic effects. Thanks to the low dose of light, it was possible to monitor the root maturation zone, where the growth and elongation of new-born root hairs and adult hairs could be observed throughout the entire experiment (Supplementary Movie S1). Single root hairs were manually selected and, after image registration, the FRET signal from a region of interest (ROI) at the root hair apex was extracted. In this case, however, although it was possible to follow the root hair growth and study the FRET variations, no relevant information about tip calcium oscillations and growth regulation mechanisms were observed because of the poor time sampling (Supplementary Fig. S2). Thus, to increase the time resolution, we reduced the interval between two subsequent acquisitions to 10 s. To avoid irradiation damage, we reduced the number of slices acquired per image to 30, with a spacing of 5 μm. This enabled the detection of tip calcium oscillations (**Fig. 2A**; Supplementary Movie S2) and the plot of the Cameleon ratio vs. time of selected ROIs corresponding to different root hairs (**Fig. 2B**). In particular, we observed a high frequency (HF) oscillation, superimposed on a lower frequency (LF) oscillation. The results of a first rough analysis of the HF oscillations were similar to those reported by Monshausen et al. (2008),

previously recorded by analyzing a single focal plane with confocal microscopy. However, the LF oscillations (the detection of which requires longer acquisition times and therefore negligible photobleaching) were not reported by the authors. We hypothesize that these LF oscillations could be related to root hair pulsatory growth. We further investigated this by following both the cpVenus (**Fig. 3A**) and the correspondent FRET ratio (**Fig. 3B**; Supplementary Movie S3) of a selected root hair that showed a marked pulsatile growth. To better evaluate the root hair elongation in a simple graphical method, we relied on kymographs (pixel line highlighted in yellow in **Fig. 3A**) of the cpVenus fluorescent channel (**Fig. 3C**). The FRET ratio images presented in **Fig. 3B** show that the calcium concentration in the apical 5 μm of the hair tip was higher, and then it quickly decreased until a lower calcium concentration was reached (Bibikova et al. 1997, Wymer et al. 1997). This gradient persisted as long as the root hair grew, oscillating in time. The FRET ratio signal, extracted after image registration, was plotted in **Fig. 3D** (corresponding to the regions highlighted at the apex of the root hair in **Fig. 3B**). The calcium signal showed a clear oscillating behavior during growth, with a period of about 5 min, associated with the pulsatory growth, as emphasized by the kymograph, which showed that the elongation of the hair was not homogeneous over time but characterized by a step-like growth, this latter being quantified in **Fig. 3D** (orange line). Moreover, in the same example, an HF signal appeared to be superimposed on the LF signal, as previously shown for the calcium signals reported in **Fig. 2B**. As a third acquisition mode, in order to better study the HF tip calcium oscillations and the
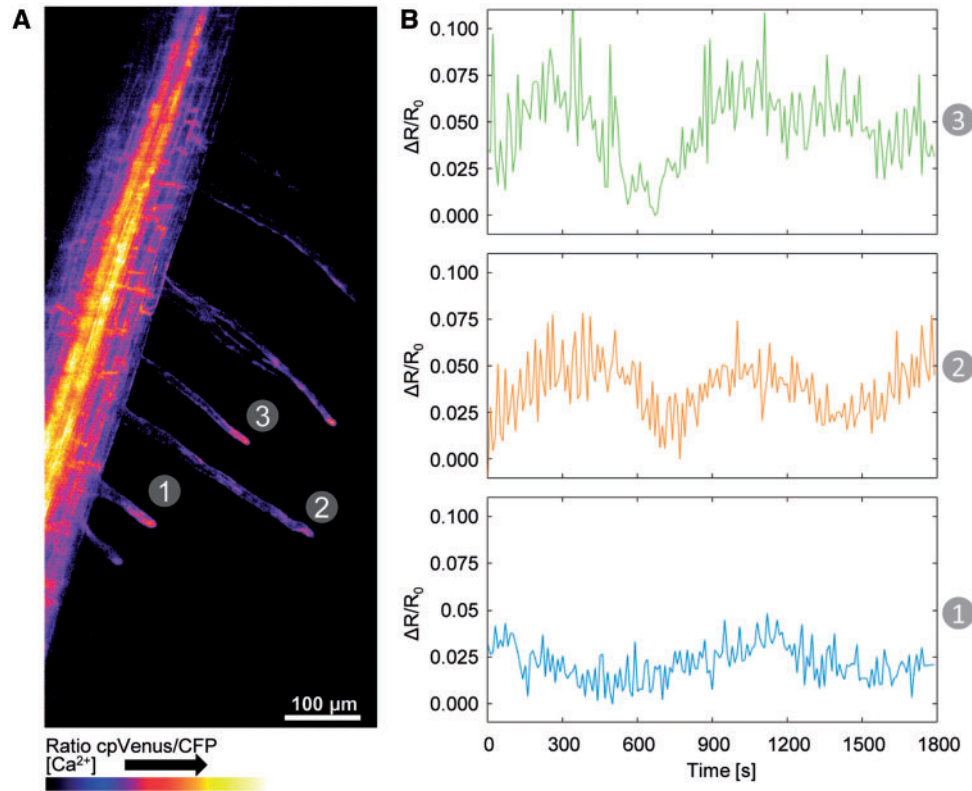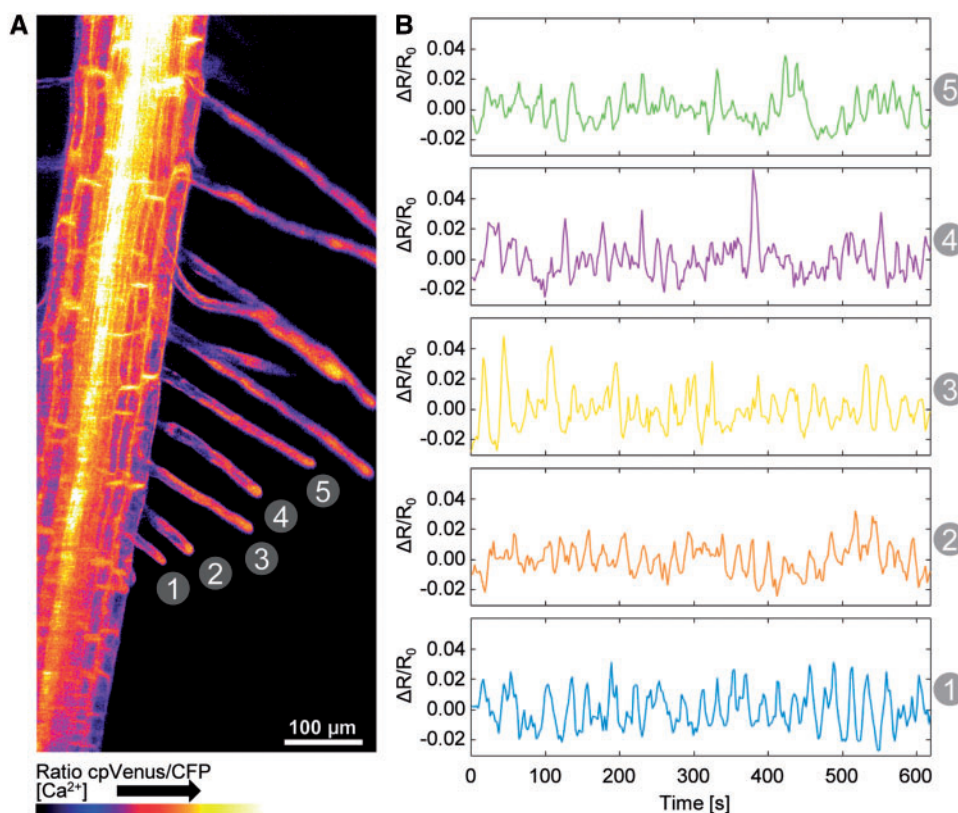
Fig. 2 MIP of the ratio between the cpVenus and CFP fluorescent channel images obtained from 30 slices of the sample spaced 5 μm apart (A). FRET signal extracted from three root hair apices evaluated as $\Delta R/R_0$ and plotted over time (B). The sampling time was 10 s and the measure was performed for 30 min.
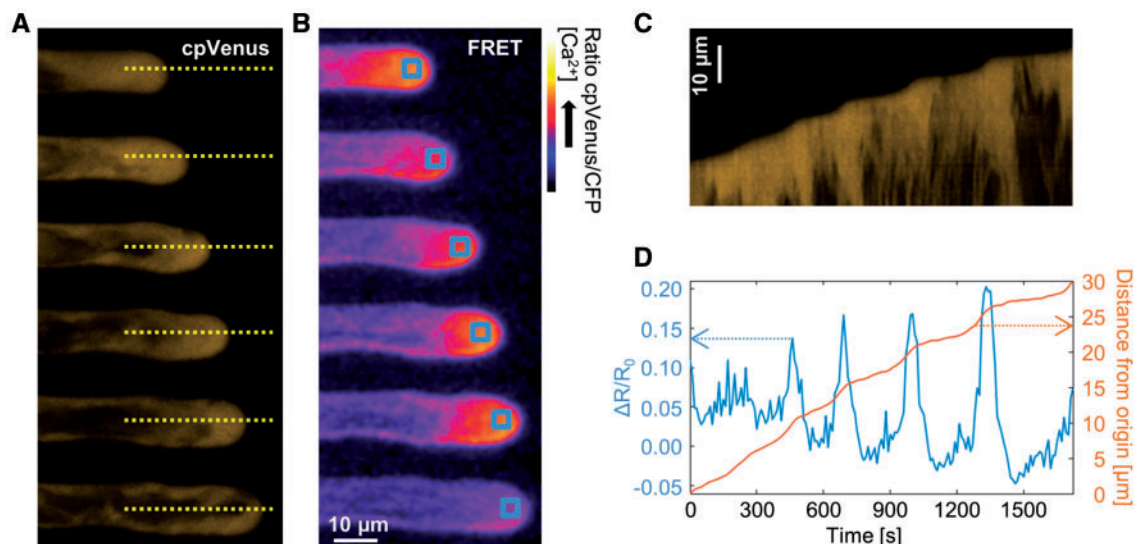
Fig. 3 Root hair pulsatory growth. MIP of a root hair from the cpVenus fluorescent channel and of the ratio images at different instants of their growth (A and B, respectively). From the cpVenus frames, by observing the temporal evolution of the pixel line highlighted in yellow, a kymograph was extracted (C), highlighting the step-like elongation. On the images of the ratio, once registered, a ROI could be selected, like that sketched in blue, and the calcium signal could be extracted (D, blue line). Moreover, the elongation can be computed as the distance of the root hair apex from its original position (D, orange line).

growth rate of root hairs, we increased the sampling rate by acquiring 3D stacks of 15 planes with a spacing of 3 μm every 3 s for 10 min. An average of five root hairs per time-lapse measurement could be imaged simultaneously in a single seedling root (**Fig. 4A, B**; Supplementary Movie S4). We imaged root hairs over a population of 12 different plants to enlarge the data set and to perform statistical analysis (as reported in **Fig. 5A**). The FRET ratio of the apex of registered root hairs still showed

Fig. 4 MIP of the ratio between the cpVenus and CFP fluorescent channels images obtained from 15 slices of the sample spaced 3 µm apart (A). FRET signal extracted from five root hair apices evaluated as $\Delta R/R_0$ and plotted over time (B). The sampling time was 3 s and the measure was repeated 270 times. The trend was removed in order to highlight the frequencies of interest.

the HF oscillations (**Fig. 4B**), with better resolution with respect to that already reported in **Figs. 2B** and **3D**. The increased sampling rate allowed us to quantify the oscillatory components precisely through Fourier analysis. Notably, the Fourier formalism allowed us to perform unbiased statistical analysis of all root hair oscillations measured from the analyzed cells in the different experiments (different seedlings). Statistical analysis of data is reported in **Fig. 5A** which shows the average of the normalized power spectral density (PSD), together with its SD. The PSD exhibited the presence of two main frequency bands corresponding to two different oscillatory components. The LF band extended from an oscillation period from 1.3 min up to 5 min (0.013 to 0.003 Hz), and roughly corresponded to the time behavior observed in the experiments presented in **Figs. 2B** and **3D**. Instead, the period of the HF oscillations ranged between 20 and 36 s (0.05 and 0.028 Hz), as shown in **Fig. 4B**. As a control, we performed the same routine analyses with ROIs drawn in the root hair shank or in the main root body (Supplementary Fig. S3A–C). In this latter case, the average PSD highlights the lack of the identified typical root hair tip oscillation frequencies (Supplementary Fig. S3D).

Growth and oscillations are correlated

The elevation in apical calcium has been shown to be essential in regulating root hair growth (Monshausen et al. 2008), similarly to that reported for pollen tubes (Felle and Hepler 1997,

Holdaway-Clarke et al. 1997). Indeed, in root hairs showing a strong pulsatile growth (such as the example shown in **Fig. 3** in which the image acquisition was at 10 s sampling), it was clearly evident that growth correlates with a tip calcium increase (**Fig. 3C, D**). Nonetheless, by following calcium variations together with the rate of growth in the plots obtained from the acquisition performed with the high sampling rate mode (3 s sampling) (**Fig. 5B**), it can be noted that the calcium peaks corresponding to the HF oscillations followed those of the growth rate. This indicates a strong temporal relationship between the variation of the cytoplasmic calcium concentration and the growth itself. A cross-correlation analysis between the calcium oscillations and the growth rates of the root hairs was therefore performed over a population of 14 root hairs from four seedlings. The average cross-correlation plotted vs. the lag showed that the calcium elevation lagged behind the peak in the growth rate by approximately 7.1 ± 0.9 s (**Fig. 5C**), in accordance with previous results from Monshausen et al. (2008).

Screening the effect of NAA in the medium along growth

In order to assess our protocol for screening the growth of seedlings under different conditions, we monitored the root hairs growth parameters of NES-YC3.6 Arabidopsis seedlings by growing them in a medium supplemented with auxin. Auxin has been reported to be the main phytohormonal
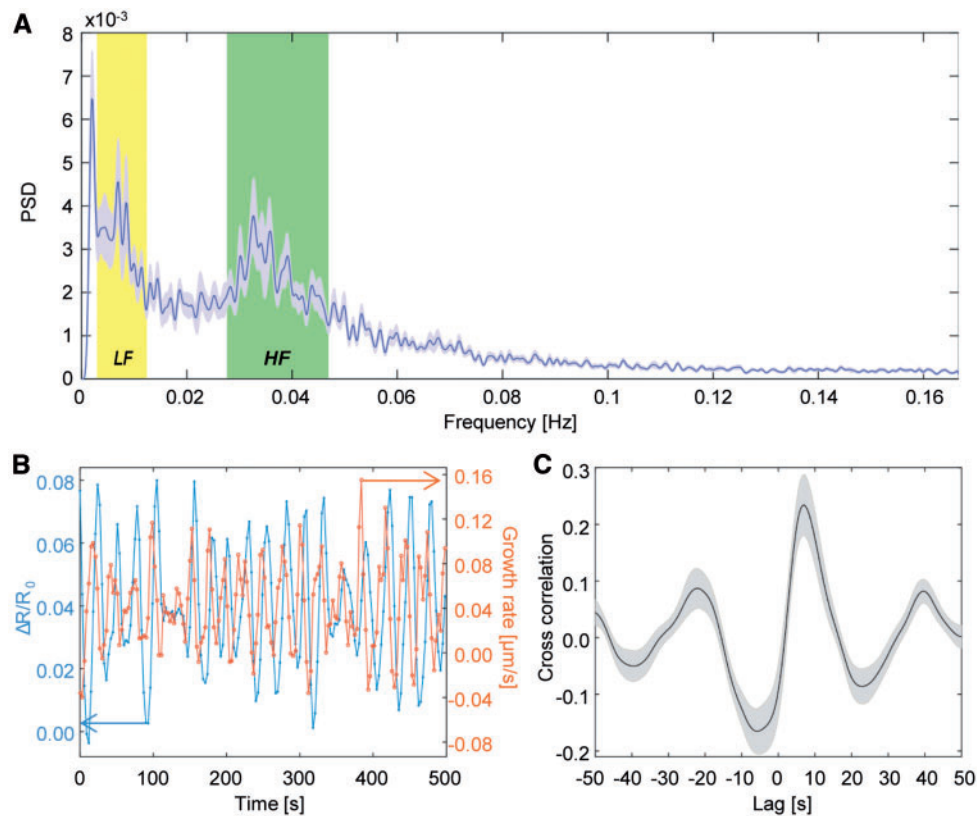
Fig. 5 Fourier analysis of the calcium oscillations extracted from root hair apices revealed a pulsatile behavior with the presence of two main bands of frequencies (LF, low frequencies, yellow background; HF, high frequencies, green background). The mean power spectral density (PSD) and the SE ($n = 43$, shaded) is reported (A). The calcium signal at high frequency (blue filled circles) from a representative root hair was plotted together with the computed rate of growth (orange open circles) of the same hair (B), the peaks of which anticipate those of the calcium concentration. Cross-correlation analysis of calcium oscillations with the rate of growth done on 14 root hairs showed that the cytosolic calcium increase lagged behind the growth rate peaks by around 7 s (C). The figure shows the average cross-correlation plotted as a function of the lag together with the SE (shaded).

regulator in root hair development (Lee and Cho 2006, Lee and Cho 2013, Velasquez et al. 2016, and references therein). Before proceeding with the LSFM analysis, we carried out an experiment with vertically grown seedlings cultivated in Petri dishes prepared with a standard Murashige and Skoog (MS/2) medium and supplemented with 50 nM 1-naphthaleneacetic acid (NAA). The lengths of roots and root hairs of 6-day-old seedlings were measured by means of a stereo microscope. Seedlings grown in the presence of 50 nM NAA showed a shorter primary root (**Fig. 6A**) and root hairs with a considerably higher average length (**Fig. 6B**). This result showed that 50 nM NAA was indeed effective in affecting the root growth apparatus in Arabidopsis, as previously reported (Lee and Cho 2006, Lee and Cho 2013, Velasquez et al. 2016, and references therein). Our next objective was to understand whether the observed increase in the average length of root hairs (**Fig. 6B**), promoted by the presence in the medium of 50 nM NAA, could depend on the direct stimulation of growth of young root hairs as well as affect calcium oscillations. We visually evaluated if the NAA effect, observed in seedlings grown in Petri dishes, could be reproduced in plants grown in the FEP tubes. Arabidopsis NES-YC3.6 seedlings germinated on standard MS/2 medium for
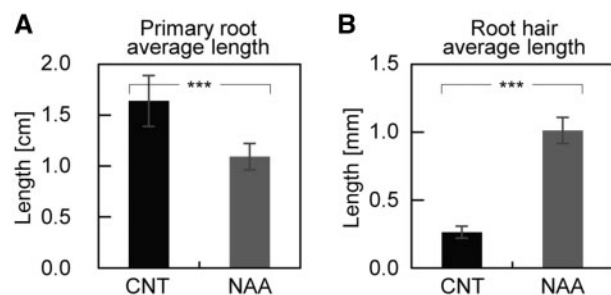
Fig. 6 Comparison between wild-type Arabidopsis seedling grown in a standard MS/2 medium or supplemented with 50 nM NAA. Primary root (A) and root hair length (B) of seedlings germinated and grown in Petri dishes in the presence or absence of 50 nM NAA. Statistical analysis shows that plants grown in the presence of NAA have, on average, a shorter primary root ($n_{CNT} = 20$ and $n_{NAA} = 18$) (A) and longer root hairs ($n_{CNT} = 23$ and $n_{NAA} = 29$) (B). Values are means ± SD.

36–40 h after vernalization were transferred to the upper edge of FEP tubes filled with standard MS/2 medium or supplemented with 50 nM NAA, and 6-day-old seedlings were visually inspected by using LSFM equipped with a ×4 objective (needed
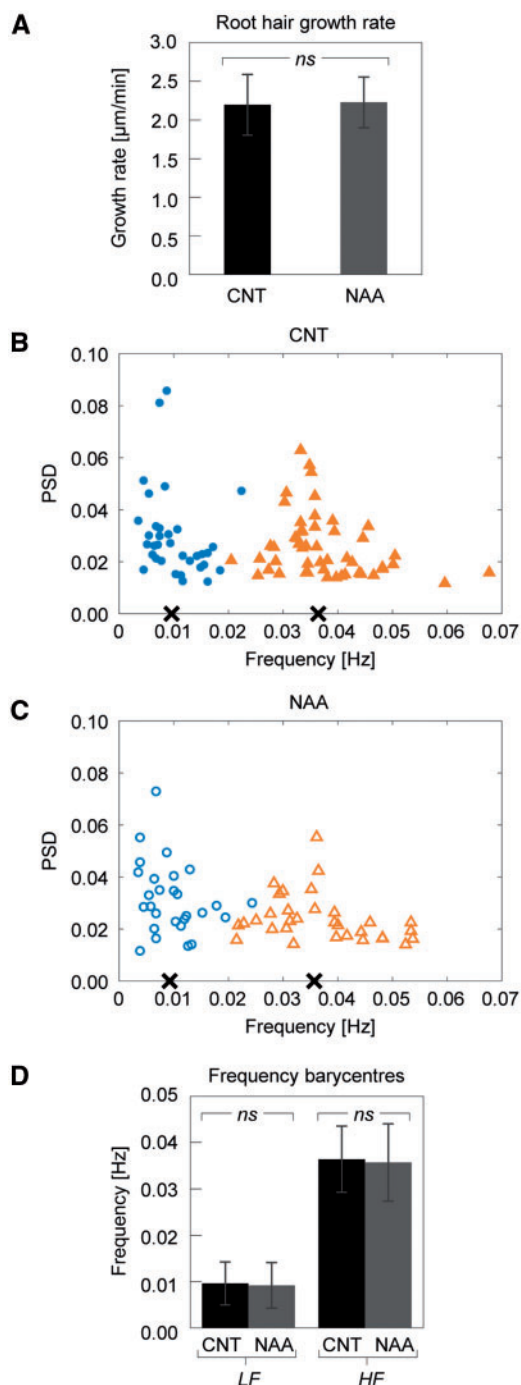
Fig. 7 Comparison of the root hair growth rate and root hair calcium oscillation frequencies present in wild-type Arabidopsis seedling grown in control conditions or in a medium supplemented with 50 nM NAA. Germinated seedlings (36–40 h after vernalization) were transferred from MS/2 standard plates to FEP tubes supplemented or not with 50 nM NAA, and seedlings were visualized after 6 d through the light sheet set-up. (A) Statistical analysis of root hair growth velocity. Values are means ± SD (n_{CNT} = 43 and n_{NAA} = 31). The two main peaks in the PSD of the control (B) and NAA-treated samples (C) (n_{CNT} = 43 and n_{NAA} = 31) were plotted and clustered through a k-mean algorithm with k = 2. The low frequency cluster is shown by blue circles, while the high frequency cluster is shown by orange triangles. Black crosses are used to visualize the computed barycenters. The mean and SE of the two main frequencies (LF, low frequency; HF, high frequency) of the two populations is presented in (D).

to increase the field of view to $3,300 \times 3,300 \, \mu m^2$) (Supplementary Fig. S 4A, B). In this latter case, since we were interested in visualizing the root apparatus only, and not extract functional growth data, we acquired images corresponding only to the emission of the cpVenus fluorescence. Representative images (of $n \geq 3$) for the two tested conditions showed that 50 nM NAA was effective in promoting the growth of the root hairs in tubes (Supplementary Fig. S4A, B). Hence, the same seedlings were analyzed by the LSFM–FRET set-up (using the ×20 objective) to evaluate the growth speed and calcium oscillations of root hairs in NAA and MS/2. Interestingly, the average growth speed of growing root hairs was the same for the two populations of plants (**Fig. 7A**), showing that NAA did not affect this parameter. We then applied the screening routine previously described for the analysis of the HF tip calcium oscillations to the control and NAA-treated seedlings. We extracted the PSD spectra for a population of 43 and 31 root hairs for the control and NAA-treated plants (**Fig. 7B, C**), respectively. Two main frequency bands could be identified for the NAA-treated population (**Fig. 7C**). In order to compare specific frequencies of the two PSDs quantitatively, we extracted the two main peaks from the PSD spectrum of each seedling, based on the a priori knowledge of the presence of two oscillatory components. The corresponding frequencies were clustered through a k-means algorithm (k = 2), which generated two clearly distinct bands (**Fig. 7B, C**). For the two identified groups of frequencies, we therefore computed the barycenters, which are equal to an oscillation period of 104 s (0.0096 Hz) and 28 s (0.036 Hz) for the control and to 111 s (0.009 Hz) and 29 s (0.035 Hz) for the NAA-treated roots. **Fig. 7D** shows the barycenter values for the two populations, with their SDs. It is evident that there was no difference between the frequencies of calcium oscillations in the two tested conditions. This is in agreement with our previous observations that the average rate of growth, which correlates with the calcium oscillations, did not change in the presence of NAA (**Fig. 7A**). To confirm this finding, we also ran a two-sample t-test on the two populations, which confirmed the null hypothesis that the two populations are equal at the 5% significance level ($P > 0.05$).

Discussion

As recently reported, LSFM can be used to record calcium dynamics in plant root cells in response to external stimuli (Costa et al. 2013). In this work, we report that the same method can be used to study spontaneous calcium oscillations in the cytosol of root hair apices. These localized calcium variations were observed in actively growing root hairs (as shown in **Fig. 5** and Supplementary Movies S1–S4), and the strict correlation between the growth of root hairs and their apical calcium elevation is an ideal subject of investigation for LSFM. Indeed, LSFM provides images of growth and the calcium dynamics of several root hairs without the need for refocusing the microscope from new-born hairs to growing and non-growing hairs. Noticeably, in contrast to traditional protocols of root and root hair

imaging (Behera and Kudla 2013, Krebs et al. 2013, Loro and Costa 2013, Zhu et al. 2014), the specific arrangement of LSFM and the designed mounting protocol allow the root hairs to grow following their 3D organization around the main root, which is left untouched during the entire measurement. In the majority of published works, imaging of root hair growth is normally run on seedling roots that are placed horizontally on a slide, thus potentially inducing perturbations to the whole plant and to root hairs themselves. Our close to physiological imaging conditions represent a considerable benefit, reducing the invasiveness of all steps required over the whole experiment. It is noted that the seedlings can live for days in FEP tubes (plants left in the tubes were able to flower; data not shown), with their survival limited only by the possible contamination of the growing medium. However, photobleaching and phototoxicity must always be taken into account in the experimental design. The light sheet technique is far less phototoxic than standard point-scanning techniques (Reynaud et al. 2008), since only a thin plane of the sample is excited and actually observed at the same time. Moreover, the flexibility of the LSFM system allowed us to design the experiments by tailoring the light dose to the phenomenon under investigation and to the time scale of interest, thus reducing phototoxicity as much as possible (Reynaud et al. 2008).

In this work, we devoted our efforts to obtaining sufficient spatial and temporal resolution to observe spontaneous cytosolic calcium oscillations in the apices of growing root hairs. To this end, we used Arabidopsis seedlings expressing the genetically encoded FRET-based calcium indicator NES-YC3.6. This calcium probe was already proved to have a sufficient dynamic range for the study of the root hair tip-focused calcium gradient (Monshausen et al. 2008). Thanks to the lateral resolution of our system ($<1\,\mu m$), which was set by the detection objective, we were able to see calcium oscillations in the tip of growing root hairs, as shown by the FRET traces in **Figs. 2B** and **4B**.

Our approach offered the possibility to generate sufficient data to perform statistical analyses of the growth parameters of root hairs. In doing so, we quantified the frequency of calcium oscillations (with Fourier analysis) from a population of root hairs (>40), and found two main frequency bands of oscillations, named here LF and HF. The first corresponded to a period of oscillation from 1.3 min to at least 5 min (correspondent to a frequency band extending from 0.013 to 0.003 Hz) and the second related to a period of oscillation of 20–36 s (frequency band spanning from 0.05 to 0.028 Hz). While the HF calcium oscillation was already reported in the literature (Monshausen et al. 2008), the LF oscillation, to the best of our knowledge, was described here for the first time and deserves more extensive investigations in the future. It is worth noting that in the average PSD of **Fig. 5A**, the position and amplitude of the first peak could have been partially influenced by the choice of the measurement time interval. Hence, the corresponding frequencies were not taken into account in the statistical analysis of the peaks. Indeed the first peak of the PSD could be due either to the presence of an even lower oscillatory behavior or to variations in the average calcium concentration gradient in the hair tip.

Moreover, it was possible to quantify the elongation of single root hairs over time and to derive their average growth rate. Note that the numerical derivation was performed after interpolating the experimental data with a spline, in order to increase the number of points digitally so as not to introduce any time shift by the derivation. The elongation was computed on the cpVenus fluorescent channel by storing the co-ordinate shifts obtained from the registration of the root hair apices in images taken at different time points. It is worth noting that, since we evaluated the root hair growth on maximum intensity projection (MIP) images, we lost the information about the elongation along the axial direction (the one set by the optical axis of the detection objective). However, when we selected the volume to be imaged, we looked for regions where root hairs were growing mainly along the propagation direction of the light sheet. Even if the displacement of the root hair apices could have been underestimated, we could clearly see peaks in the growth rate. Moreover, neither the frequencies nor the correlations estimated in our study, which are indeed our main findings, were affected. In fact, since the projection of the lengths along the line of sight affected all the measurements in the same way, the frequency peaks found through Fourier analysis and correlations depended only on the time course of the elongation signals. Hence, we could still see pulses in the growth of the root hairs. Fast oscillations of the cytosolic calcium gradient present in the tip of root hairs were previously found to correlate with the step-like growth (Monshausen et al. 2008). We confirmed this result on a population of 14 root hairs, by cross-correlating the FRET signal with the growth rate. The FRET peaks lag behind the maxima of the growth rate by 7 s, hence the tip calcium increase appears to follow the pulsatile growth of the root hair, and does not precede it. This latter observation confirms data published by Monshausen et al. (2008) and also supports studies carried out in growing pollen tubes in which the tip calcium peaks clearly lag behind pulsatile growth (Holdaway-Clarke et al. 1997, Winship et al. 2017).

Based on our data, we point out that our method offers an approach to measure the parameters of root hair growth in Arabidopsis. This allowed us to collect a sufficient number of replicas that facilitated the comparison of root hair growth parameters between treatments and different genotypes. In Petri dishes, the presence of 50 nM NAA, on average, determined the development of a shorter primary root and longer root hairs compared with control plants. Thus, we monitored the growth parameters of root hairs in Arabidopsis seedlings growing in FEP tubes in control conditions or in a medium supplemented with 50 nM NAA in time-lapse experiments by LSFM. Since calcium oscillation and growth rate are linked, it could be thought that auxin, which participates in the increase of the root hair length, would also influence both the rate of growth and the frequency of oscillation of the calcium signal. However, our analysis showed that there is no statistically significant difference in the PSD of the calcium time course in young root hairs for the two populations of plants. Both populations showed two main frequency bands with the same barycenters that correspond to a period of around 28 s for the high frequency. This is in agreement with our observations that the rate of growth did not change in the presence of NAA.

Even though NAA has an effect on the average growth of the root hairs, which appeared to be longer, it did not impact the velocity of growth, but took part in a different regulating mechanism. The absence of an effect of NAA on the growth parameters of young root hairs is, in our opinion, an interesting observation per se and it does not contrast with the proposed model in which the auxin-induced increased root hair length is dependent on the increased expression time of the RSL4 transcription factor. In fact constitutive expression, in Arabidopsis plants, of RSL4 determines a longer growth (Yi et al. 2010, Datta et al. 2015, Vijayakumar et al. 2016). However, even if we failed to observe changes in root hair growth parameters with NAA, we believe that this technique will facilitate studies of root hair development in different genetic backgrounds (e.g. *Atrbohc*; Foreman et al. 2003, Grierson et al. 2014) or in tests of the effects of stimuli, such as low phosphate or low nitrogen (Bates and Lynch 1996, Müller and Schmidt 2004, Grierson et al. 2014), which are known to affect root hair growth.

In conclusion, the presented protocol offers a solution for short- and long-term studies of root hair growth with associated tip calcium oscillations, with minimal perturbation introduced by the researcher.

Materials and Methods

Arabidopsis seedling preparation

Seeds of *A. thaliana* Col-0 were surface sterilized by vapor-phase sterilization (Clough and Bent 1998) and plated on MS/2 medium (MS including vitamins; Duchefa) (Murashige and Skoog 1962) supplemented with 0.1% (w/v) sucrose, 0.05% (w/v) MES, pH 5.8 adjusted with KOH and solidified with 0.8% (w/v) plant agar (Duchefa). After stratification at $4\,°C$ in the dark for 2–3 d, seeds were transferred to the growth chamber with 16/8 h cycles of light (70 µmol $m^{-2}\,s^{-1}$) at $24\,°C$.

To carry out the measurement of root and root hair length in Petri dishes, Arabidopsis seedlings were grown on the standard medium jellified with 0.5% Phytagel^{TM} (w/v) (Duchefa) or supplemented with the auxin NAA with a final concentration of 50 nM. Six-day-old vertically grown seedlings were analyzed for the measurements of the root and root hair length using a stereo microscope (Leica MZ10 F) equipped with a CCD camera (Leica). The root and root hair length was measured on the acquired images with Fiji (https://fiji.sc/): an open-source platform for biological image analysis (Schindelin et al. 2012).

Phytagel- and agar-based solution preparation

FEP (Adtech FT2×3) tubes with an internal diameter of 0.8 mm and manually cut into 3 cm long pieces using a razor blade, were cleaned first with 1 M NaOH, then with a diluted NaOH solution (0.5 M) and finally with 70% ethanol. After washing with 1 M NaOH, a 10 min sonication was performed at each cleaning step. The tubes were then rinsed with MilliQ water and coupled with the head of a 10 µl pipette tip (manually cut), placed into cleaned pipette tip boxes and afterwards autoclaved at $121\,°C$ for 20 min. The FEP tubes were then filled with the MS/2 medium used for the seed germination but in this case jellified with 0.5% Phytagel^{TM} (w/v) (Duchefa) instead of plant agar (Maizel et al. 2011). The tubes were filled from the bottom using a P200 micropipette. To prevent the evaporation of water from the Phytagel^{TM}-based medium, the top of the tubes was covered with a plant agar-based medium plug, thus creating a small cap. After solidification, a sterilized bistoury was used to remove the excess cap medium. NAA was added to the medium with a final concentration of 50 nM and before the preparation of the tubes. After seedling germination and fluorescence inspection, we quickly moved the fluorescent seeds from the plate to the top of the tubes (to avoid root drying), using sterilized pliers and without clamping them. We placed seedlings over the top of the tubes, so

the plantlets could grow inside the filled tubes. The tubes were transferred to a tip box that was finally filled with MS/2 liquid medium without sucrose and sealed to avoid contamination. The mounting procedure and the special illumination and detection configuration of LSFM allowed the seedlings to be held from the top of the chamber in a vertical position, with the roots growing directly in the jellified medium inside the transparent tubes. Hence, there was no need to transfer the specimen to the microscope slide during time-lapse measurements, and no sample manipulation was necessary. To mount the tubes with the plant in the imaging chamber, we designed a special holder. It consists of a hollow aluminum tube in which a pipette tip can be stuck. It is possible to shine white light during daytime through the inner cavity, while measurements are not being performed. There are also lateral holes for letting air reach the shoot. When plants were ready to be imaged, we plugged the pipette tip with the tube into the hollow tube, and quickly moved the whole holder to the imaging chamber, fixing it on a rotation and translation stage for positioning of the sample. It must be noted that for root hair growth analyses the plant could be imaged through the tube itself, providing a strong specimen stability for several hours to days (data not shown).

LSFM set-up for FRET measurement

The light sheet set-up implemented is a LSFM with single-sided illumination and detection (Supplementary Fig. S1). The system has been designed to be easy to use even by inexpert users, for routine screening of a large number of samples with almost no need for realignment. The output of a single-mode fiber, coupled to a laser emitting at 442 nm (MDL-III-442, CNI), is collimated and then focalized through a cylindrical lens (f_{CL} = 50 mm) in a horizontal plane. A 1× telescope ($f_1 = f_2$ = 50 mm; Thorlabs) conjugates the focal plane of the cylindrical lens to the back focal plane of a ×10 water-dipping microscope objective [numerical aperture (NA) = 0.3, UMPLFLN 10XW; Olympus], which provides a vertical light sheet in its front focal plane, matching the field of view of the observation objective. The detection stage is composed of a ×20 water-dipping microscope objective (NA = 0.5, UMPLFLN 20XW; Olympus) held orthogonally to the excitation axis. Since the calcium indicator is FRET based, a two-wavelength detection is needed. Thanks to the vertical geometry of plant roots, it is practical to record two images with different spectral content on the same pixelated detector by splitting the detection path into two spectral channels. The immersion objective is followed by a ×1 relay lens system ($f_3 = f_4$ = 100 mm; Thorlabs), the intermediate image plane of which is exploited to position a vertical slit. The horizontal dimension of the slit is 400 µm, exactly half of the field of view. A dichroic filter at 505 nm (DMLP505; Thorlabs) creates two-color replicas of the sample image, which are then sent through two band-pass filters (MF479-40 and MF535-22 emission filters; Thorlabs) and a tube lens (U-TLU-1-2; Olympus) by two broadband mirrors (BBSQ1-E02; Thorlabs). The tube lens creates the images of the CFP and the cpVenus fluorescent signals on the two sides of the CMOS sensor (Neo 5.5 sCMOS, 2,560 × 2,160 pixels; ANDOR). The laser power was set to 20 µW on the sample, which proved not to give any relevant photobleaching during illumination over the half hour experiment. To minimize the light dose to the sample, an automatic shutter switch opens the laser beam only when the camera is in acquisition mode. A white LED illuminator in transmitted light configuration is used for sample alignment to avoid unnecessary excitation of the specimen. The sample is held vertically in a custom-made 3D printed chamber, filled with the growing medium of the plants. The sample is then scanned along the detection axis to acquire 3D stacks of images through a motorized translation stage (PI M-405.CG). The camera acquisition, sample translation stage and shutter are synchronized via home-made LabVIEW software. This software permits the observation of the two channels, to visualize their ratio in real time and to record the data. In terms of sectioning capability, the beam waist of the light sheet was characterized by means of fluorescent beads (0.1 µm diameter, Molecular Probes) suspended in 1% agarose at a low concentration (1 : 4,000). The light sheet waist was found to be 2.6 µm thick, meaning that the Rayleigh range is 48 µm, around half the diameter of a sample plant root.

Large field imaging

A light sheet configuration for large field image acquisition of the growing seedlings was also used (Supplementary Fig. S3A, B). In this case, a long working distance ×4 objective was used for the detection. The signal was directly sent to

a second camera (ORCA Flash 4.0; Hamamatsu) provided with a tube lens (U-TLU-1-2; Olympus). A more detailed description of this system can be found in Candeo et al. (2016).

3D measurement of the development of multiple root hairs

Before time-lapse measurements, a morphological inspection of the sample was performed by recording the cpVenus fluorescence from 300 planes spaced 1.5 μm apart, with a field of view of $800\times450\,\mu m^2$. The 3D reconstruction of the whole plant root was then obtained from the image stack with the Fiji plugin '3D viewer' (https://fiji.sc/).

Acquisition

The acquisition parameters were set after performing test experiments to assess the photobleaching of the calcium probe. Since many experiments are run on a daily basis, it is also convenient to consider the data set dimension. A trade-off between the number of acquired planes and their spacing is indeed necessary. Moreover, it is imperative that the time to acquire and save one image stack does not exceed the sampling time necessary to observe the phenomenon of interest. It is worth mentioning that the camera is acquiring while the sample is moving smoothly. This strategy avoids the settling time of the translation stage in a stepping regime, allows the rapid recording of the 3D data set and prevents sample vibrations. Note that the translation step within the acquisition time could be larger than the light sheet, thus increasing the thickness of the sections. Long-term acquisitions of 5 h were made by acquiring a stack of 100 images with an axial step of 3 μm every 3 min. In this case, we binned 2×2 times the image (to reduce the amount of saved data) and used an exposure time of 50 ms per plane. Acquisitions aimed to record low frequency calcium oscillations were performed recording 30 planes with a spacing of 5 μm, and an exposure time of 100 ms per plane. We acquired one stack every 10 s for 30 min. The axial step was increased in order to reduce the light dose impinging on the sample, while still obtaining an acceptable axial resolution. Fast imaging of root hair calcium oscillations was done by recording 270 time points every 3 s, acquiring 15 planes spaced 3 μm apart. The exposure time was set to 100 ms. When we acquired only part of the volume of the plant, we focused our attention on one side of the root (the one closer to the illumination objective) and tried to image as many root hairs as possible. A general problem of LSFM is the huge amount of data produced: a typical stack of 30 planes acquired at 270 time points produced approximately 80 Gbyte of data for each sample. In order to facilitate the analysis of this data set, we did not store the entire stack but only two images, representative of each acquired time point. These images were the MIP of the stack, which was used for visualization purpose, and the sum (average) of the stack, which was used for quantification of the calcium oscillations. This approach has the drawback of losing the 3D information of the data set (see the Discussion), but was still effective for thin root hairs, that are the focus of this study. In order to observe the more complex structure of the plant root, more advanced data storage and processing methods would be required. In detail, in the time-lapse experiments we normally saved the MIP and the sum images of the CFP and cpVenus fluorescent channels, and the MIP of the ratio between the two channels calculated after background subtraction. These five images were stored directly during the acquisition.

Root hair registration and growth analysis

In order to quantify the lateral root hair growth, we applied a semi-automatic routine to register the image stacks taken at different times. For this purpose, we calculated the MIP of the cpVenus fluorescence for every time point. An ROI around every root hair was selected by hand. The registration of each ROI was performed by computing the cross-correlation between each couple of consecutive MIPs, in order to maintain the root hair apex at the same position. This computation was performed with the Fiji plugin 'Template Matching' (https://sites.google.com/site/qingzongtseng/template-matching-ij-plugin) after selecting the root hair apex as a landmark and using a subpixel cross-correlation method. The horizontal and vertical displacements were then stored and the process was iterated for all time points. The instantaneous hair growth was computed by tracking the position of the root hair apex through the Pythagorean theorem, taking into account the pixel size and the spacing

between adjacent planes. To estimate the instantaneous growth velocity, it is necessary to compute the derivative of the growth. However, by doing so, the growth velocity would be shifted by one-half of the sampling time. We interpolated the experimental points of the hair growth using a spline method with cubic interpolation. We then calculated the derivative of this new function and obtained the growth rate.

Kymograph

A graphical method to evaluate the root hair elongation relies on a kymograph. This tool gives a space–time representation of the evolution of the pixel corresponding to the tip of a root hair observed in an image sequence ($x, y; t$). The pixel columns at the center of the hair for each time point MIP were stitched together side by side to create a new image, which depicts the temporal evolution of the hair elongation thorough the Fiji Dynamic Reslice function. To extract the growth velocity, the kymograph must be converted into a binary image by setting a threshold. By counting all the pixels in the vertical axis and multiplying them by the size of a pixel, the profile can be converted into the instantaneous displacement of the root hair tip and, after a derivative operation, into the instantaneous growth velocity.

Calcium variation evaluation

Calcium analyses were performed on the ratio images from the simultaneously acquired cpVenus and CFP channels. The ratio image from single slices, as well as the image of the ratio of the sum of all the slices, were saved directly during the acquisition. The same ROIs used for image registration were used for the root hair selection. These ROIs were registered using the same shift co-ordinates found for the registration of the cpVenus fluorescent channel. A second ROI was drawn around the apical calcium gradient and the average fluorescence signal inside the ROI was extracted. We computed the FRET variation as $\Delta R/R_0$, i.e. the ratio between the emission of the cpVenus and the CFP:

$$\frac{\Delta R}{R_0} = \frac{\frac{cpVenus}{CFP} - \frac{cpVenus_0}{CFP_0}}{\frac{cpVenus_0}{CFP_0}}$$

and plotted it over time (Supplementary Fig. S5). The main trend of the FRET signal time course was removed before analysis.

Fourier analysis of spontaneous calcium oscillations

The Fourier analysis was used to determine the main frequencies in the observed calcium oscillations. The Fourier transform decomposes a signal into the sum of sinusoids. For time domain signals that are sampled at N equally spaced time points, the discrete version of the Fourier transform must be used, which is defined as follows:

$$G(f_k) = \sum_{n=1}^{N} g(t_n) e^{-\frac{i2\pi kn}{N}} \quad k = 1 - \frac{N}{2}, \ldots, \frac{N}{2}$$

where $g(tn)$ represents the time samples of the signal, $G(fk)$ represents the samples of the Fourier transform in the frequency domain, and $e{-}i^2\pi kn/N$ is a function having both a real and an imaginary part. The discrete Fourier transform $G(fk)$ has the same number of samples N of the signal $g(tn)$, while the sampling intervals in the frequency (Δf) and time (Δt) domains are related to each other by the simple equation $\Delta f =1/N\Delta t$. To avoid aliasing, i.e. an improper ascription of higher frequency components to lower ones, the sampling rate ($1/\Delta t$) must be greater than, or equal to, twice the highest frequency present in the recorded signal, as stated by the Nyquist sampling theorem. We converted the sequences of time samples to the frequency domain by applying the discrete Fourier transform, which is computed through a built-in MATLAB function. The frequency resolution was digitally increased by padding the end of the time series with zeroes up to a number of elements equal to a power of 2. To identify and quantify oscillatory patterns within the calcium recordings, we calculated the power spectrum $P(fk)$, defined as:

$$P(f_k) = \frac{1}{N} |G(f_k)|^2.$$

A peak in the power spectrum indicates the existence of a major harmonic component in the recording.

Autocorrelation for periodicity investigation in a single calcium signal

The correlation of a signal with itself is an effective tool to reveal repeating patterns and, in particular, periodic behavior. The discrete autocorrelation operator was applied to our data sequences to achieve the correlation function ρk, normalized to unit:

$$\rho k = \frac{\sum_{i=1}^{N-k}(X_i - \overline{X})(X_{i+k} - \overline{X})}{\sum_{i=1}^{N}(X - \overline{X})^2} \, k = 0, 1, \ldots, N-1$$

where X_i is the ith data point, $\overline{X}$ is the mean of all N data points. X_{i+k} is the ith data point shifted by k sampling intervals Δt. In general, one or more peaks in the correlation function imply that the data exhibit periodicity, since the temporally shifted replica overlaps with the original signal after a lag multiple of k Δt. The built-in MATLAB function 'xcorr' can be exploited for this purpose.

Cross-correlation between calcium oscillations and growth rate

The cross-correlation can be used to measure the similarity between two signals. To show the relationship between the growth pulses of the root hairs and the calcium oscillations, we performed the cross-correlation analysis between these two data sets. The cross-correlation between two signals X and Y, sampled at N time points, is given by:

$$R_m = \sum_{i=1}^{N-|m|}(X_i - \overline{X})(Y_{i-m} - \overline{Y}), \; m = -(N-1), \ldots, N-1.$$

where X_i is the ith sample of the variable X, Y_{i-m} is the corresponding time-shifted sample of the variable Y, and $\overline{X}$ and $\overline{Y}$ are the respective mean values. To evaluate the cross-correlation between the growth pulses and the calcium oscillations, we used the same MATLAB function 'xcorr', which changes its behavior according to the arguments. Finally, the cross-correlation was plotted as a function of lag. The presence of a sharp peak in the graph indicates that the two signals are 'strongly' correlated, i.e. they become similar to each other upon a time shift. The position of the peak gives the delay of the signal Y with respect to X, while its amplitude gives the degree of correlation ($-1 < R_m < 1$).

Separating high and low frequency oscillation contributions

To partition the different frequency contributions into unbiased clusters, we used a k-means algorithm implemented in MATLAB with cityblock distance. We chose the arrangement that minimized the distance out of 10 different random initializations. To find the appropriate number of clusters k, an automatic sweep with k between 2 and 10 was run. The results were inspected with silhouette plots, which showed that the best arrangement was the one with $k = 2$. The representative value for each cluster was found as the barycenter of the cloud of frequencies, weighted with the PSD amplitude.

Comparison between control plants and plants with modified medium

To compare the control and NAA-treated seedlings statistically, we first verified that for each frequency the distribution was normal by plotting the corresponding histogram. We used a two-sample t-test to test the null hypothesis that the PSD of the populations came from independent random samples from normal distributions with equal means and equal but unknown variances with a 5% significance level.

Supplementary data

Supplementary data are available at PCP online.

Disclosures

The authors have no conflicts of interest to declare.

References

Balcerowicz, D., Schoenaers, S. and Vissenberg, K. (2015) Cell fate determination and the switch from diffuse growth to planar polarity in Arabidopsis root epidermal cells. *Front. Plant Sci.* 6: 1163.

Band, L.R., Wells, D.M., Larrieu, A., Sun, J., Middleton, A.M., French, A.P., et al. (2012) Root gravitropism is regulated by a transient lateral auxin gradient controlled by a tipping-point mechanism. *Proc. Natl. Acad. Sci. USA* 109: 4668–4673.

Bassi, A., Schmid, B. and Huisken, J. (2015) Optical tomography complements light sheet microscopy for in toto imaging of zebrafish development. *Development* 142: 1016–1020.

Bates, T.R. and Lynch, J.P. (1996), Stimulation of root hair elongation in *Arabidopsis thaliana* by low phosphorus availability. *Plant Cell Environ.* 19: 529–538.

Behera, S. and Kudla, J. (2013) High-resolution imaging of cytoplasmic Ca^{2+} dynamics in Arabidopsis roots. *Cold Spring Harb. Protoc.* 2013: 665–669.

Berthet, B. and Maizel, A. (2016) Light sheet microscopy and live imaging of plants. *J. Microsc.* 263: 158–164.

Bibikova, T.N., Zhigilei, A. and Gilroy, S. (1997) Root hair growth in *Arabidopsis thaliana* is directed by calcium and an endogenous polarity. *Planta* 203: 495–505.

Campanoni, P. and Blatt, M.R. (2007) Membrane trafficking and polar growth in root hairs and pollen tubes. *J. Exp. Bot.* 58: 65–74.

Candeo, A., Sana, I., Ferrari, E., Maiuri, L., D'Andrea, C., Valentini, G., et al. (2016) Virtual unfolding of light sheet fluorescence microscopy dataset for quantitative analysis of the mouse intestine. *J. Biomed. Opt.* 21: 56001.

Charpentier, M. and Oldroyd, G.E.D. (2013) Nuclear calcium signaling in plants. *Plant Physiol.* 163: 496–503.

Clough, S.J. and Bent, A.F. (1998) Floral dip: a simplified method for Agrobacterium-mediated transformation of *Arabidopsis thaliana*. *Plant J.* 16: 735–743

Coelho, S.M., Brownlee, C. and Bothwell, J.H. (2008) A tip-high, $Ca^{(2+)}$-interdependent, reactive oxygen species gradient is associated with polarized growth in *Fucus serratus* zygotes. *Planta* 227: 1037–1046.

Costa, A., Candeo, A., Fieramonti, L., Valentini, G. and Bassi, A. (2013) Calcium dynamics in root cells of *Arabidopsis thaliana* visualized with selective plane illumination microscopy. *PLoS One* 8: e75646.

Costa, A. and Kudla, J. (2015) Colorful insights: advances in imaging drive novel breakthroughs in Ca^{2+} signaling. Mol. Plant 8: 352–355.

Datta, S., Prescott, H. and Dolan, L. (2015) Intensity of a pulse of RSL4 transcription factor synthesis determines Arabidopsis root hair cell size. Nat. Plants 1: 15138.

Feijó, J.A., Costa, S.S., Prado, A.M., Becker, J.D. and Certal, A.C. (2004) Signalling by tips. Curr. Opin. Plant. Biol. 7: 589–598.

Felle, H.H. and Hepler, P.K. (1997) The cytosolic Ca^{2+} concentration gradient of Sinapis alba root hairs as revealed by Ca^{2+}-selective microelectrode tests and fura–dextran ratio imaging. Plant Physiol. 114: 39–45.

Foreman, J., Demidchik, V., Bothwell, J.H., Mylona, P., Miedema, H., Torres, M.A., et al. (2003) Reactive oxygen species produced by NADPH oxidase regulate plant cell growth. Nature 422: 442–446.

Franklin-Tong, V.E. (1999) Signaling and the modulation of pollen tube growth. Plant Cell 11: 727–738.

Gilroy, S. (1997) Fluorescence microscopy of living plant cells. Annu. Rev. Plant Physiol. Plant Mol. Biol. 48: 165–190.

Grierson, C., Nielsen, E., Ketelaarc, T. and Schiefelbein, J. (2014) Root hairs. Arabidopsis Book 12: e0172.

Holdaway-Clarke, T.L., Feijo, J.A., Hackett, G.R., Kunkel, J.G. and Hepler, P.K. (1997) Pollen tube growth and the intracellular cytosolic calcium gradient oscillate in phase while extracellular calcium influx is delayed. Plant Cell 9: 1999–2010.

Kao, F.S. and Chen, T.-M. (2002) A study on the luminescent properties of new green-emitting terbium-activated $CaIn_2O_4{:}xTb$ phosphors. J. Luminesc. 96: 261–267.

Keinath, N.F., Waadt, R., Brugman, R., Schroeder, J.I., Grossmann, G., Schumacher, K., et al. (2015) Live cell imaging with R-GECO1 sheds light on flg22- and chitin-induced transient $[Ca^{(2+)}]_{cyt}$ patterns in Arabidopsis. Mol. Plant 8: 1188–2000.

Kim, H.S., Czymmek, K.J., Patel, A., Modla, S., Nohe, A., Duncan, R., et al. (2012) Expression of the Cameleon calcium biosensor in fungi reveals distinct $Ca^{(2+)}$ signatures associated with polarized growth, development, and pathogenesis. Fungal Genet. Biol. 49: 589–601.

Konrad, K.R., Wudick, M.M. and Feijó, J.A. (2011) Calcium regulation of tip growth: new genes for old mechanisms. Curr. Opin. Plant Biol. 14: 721–30.

Krebs, M, Held, K., Binder, A., Hashimoto, K., Den Herder, G., Parniske, M., et al. (2012) FRET-based genetically encoded sensors allow high-resolution live cell imaging of Ca^{2+} dynamics. Plant J. 69: 181–192.

Lange, M. and Peiter, E. (2016) Cytosolic free calcium dynamics as related to hyphal and colony growth in the filamentous fungal pathogen Colletotrichum graminicola. Fungal Genet. Biol. 91: 55–65.

Lee, R.D. and Cho, H.T. (2013) Auxin, the organizer of the hormonal/environmental signals for root hair growth. Front. Plant Sci. 4: 448.

Lee, S.H. and Cho, H.T. (2006) PINOID positively regulates auxin efflux in Arabidopsis root hair cells and tobacco cells. Plant Cell 18: 1604–1616.

Loro, G. and Costa, A. (2013) Imaging of mitochondrial and nuclear Ca^{2+} dynamics in Arabidopsis roots. Cold Spring Harb. Protoc. 2013: 781–785.

Maizel, A., von Wangenheim, D., Federici, F., Haseloff, J. and Stelzer, E.H.K. (2011) High-resolution live imaging of plant growth in near physiological bright conditions using light sheet fluorescence microscopy. Plant J. 68: 377–385.

Mendrinna, A. and Persson, S. (2015) Root hair growth: it's a one way street. F1000Prime Rep. 7: 23.

Michard, E., Alves, F. and Feijó, J.A. (2009) The role of ion fluxes in polarized cell growth and morphogenesis: the pollen tube as an experimental paradigm. Int. J. Dev. Biol. 53: 1609–1622.

Miyawaki, A., Llopis, J., Heim, R., McCaffery, J.M., Adams, J.A., Ikura, M., et al. (1997) Fluorescent indicators for Ca^{2+} based on green fluorescent proteins and calmodulin. Nature 388: 882–887.

Monshausen, G.B., Bibikova, T.N., Messerli, M.A., Shi, C. and Gilroy, S. (2007) Oscillations in extracellular pH and reactive oxygen species modulate tip growth of Arabidopsis root hairs. Proc. Natl. Acad. Sci. USA 104: 20996–21001.

Monshausen, G.B., Messerli, M.A. and Gilroy, S. (2008) Imaging of the Yellow Cameleon 3.6 indicator reveals that elevations in cytosolic Ca^{2+} follow oscillating increases in growth in root hairs of Arabidopsis. Plant Physiol. 147: 1690–1698.

Müller, M. and Schmidt W. (2004) Environmentally induced plasticity of root hair development in Arabidopsis. Plant Physiol. 134: 409–419.

Murashige, T. and Skoog, F. (1962) A revised medium for rapid growth and bioassays with tobacco tissue cultures. Physiol. Plant. 15: 473–497.

Nagai, T., Yamada, S., Tominaga, T., Ichikawa, M. and Miyawaki, A. (2004) Expanded dynamic range of fluorescent indicators for Ca^{2+} by circularly permuted yellow fluorescent proteins. Proc. Natl. Acad. Sci. USA 101: 10554–10559.

Okumoto, S., Jones, A. and Frommer, W.B. (2012) Quantitative imaging with fluorescent biosensors. Annu. Rev. Plant Biol. 62: 273–297.

Reynaud, E.G., Krzic, U., Greger, K. and Stelzer, E.H. (2008) Light sheet-based fluorescence microscopy: more dimensions, more photons, and less photodamage. HFSP J. 2: 266–275.

Rounds, C.M. and Bezanilla, M. (2013) Growth mechanisms in tip-growing plant cells. Annu. Rev. Plant Biol. 64: 243–265.

Schindelin, J, Arganda-Carreras, I., Frise, E., Kaynig, V., Longair, M., Pietzsch, T., et al. (2012) Fiji: an open-source platform for biological-image analysis. Nat. Methods 9: 676–682.

Swanson, S.J., Choi, W.G,. Chanoca, A. and Gilroy S. (2011) In vivo imaging of Ca^{2+}, pH, and reactive oxygen species using fluorescent probes in plants. Annu. Rev. Plant Biol. 62: 273–297.

Velasquez, S.M., Barbez, E., Kleine-Vehn, J. and Estevez, J.M. (2016) Auxin and cellular elongation. Plant Physiol. 170: 1206–1215.

Véry, A.A. and Davies, J.M. (2000) Hyperpolarization-activated calcium channels at the tip of Arabidopsis root hairs. Proc. Natl. Acad. Sci. USA 97: 9801–9826.

Vijayakumar, P., Datta, S. and Dolan, L. (2016) ROOT HAIR DEFECTIVE SIX-LIKE4 (RSL4) promotes root hair elongation by transcriptionally regulating the expression of genes required for cell growth. New Phytol. 212: 944–953.

Winship, L.J., Rounds, C. and Hepler, P.K. (2017) Perturbation analysis of calcium, alkalinity and secretion during growth of lily pollen tubes. Plants 6: 3.

Wymer, C.L., Bibikova, T.N. and Gilroy, S. (1997) Cytoplasmic free calcium distributions during the development of root hairs of Arabidopsis thaliana. Plant J. 12: 427–439.

Yan, A., Xu, G., and Yang, Z.-B. (2009) Calcium participates in feedback regulation of the oscillating ROP1 Rho GTPase in pollen tubes. Proc. Natl. Acad. Sci. USA 106: 22002–22007.

Yi, K., Menand, B., Bell, E. and Dolan, L. (2010) A basic helix–loop–helix transcription factor controls cell growth and size in root hairs. Nat. Genet. 42: 264–267.

Zhu, X., Taylor, A., Zhang, S., Zhang, D., Feng, Y., Liang, G., et al. (2014) Measuring spatial and temporal Ca^{2+} signals in Arabidopsis plants. J. Vis. Exp. 91: e51945.